Photosynth Res (2006) 90:111–123
DOI 10.1007/s11120-006-9098-0

REGULAR PAPER

Imaging viral infection: studies on *Nicotiana benthamiana* plants infected with the pepper mild mottle tobamovirus

María Luisa Pérez-Bueno · Massimo Ciscato · Martin vandeVen · Isabel García-Luque · Roland Valcke · Matilde Barón

Received: 13 March 2006 / Accepted: 18 August 2006 / Published online: 3 January 2007

Abstract We have studied by kinetic Chl-fluorescence imaging (Chl-FI) *Nicotiana benthamiana* plants infected with the Italian strain of the pepper mild mottle tobamovirus (PMMoV-I). We have mapped leaf photosynthesis at different points of the fluorescence induction curve as well as at different post-infection times. Images of different fluorescence parameters were obtained to investigate which one could discriminate control from infected leaves in the absence of symptoms. The non-photochemical quenching (NPQ) of excess energy in photosystem II (PSII) seems to be the most adequate chlorophyll fluorescence parameter to assess the effect of tobamoviral infection on the chloroplast. Non-symptomatic mature leaves from inoculated plants displayed a very characteristic time-varying NPQ pattern. In addition, a correlation between NPQ amplification and virus localization by tissue-print was found, suggesting that an increase in the local NPQ values is associated with the areas invaded by the pathogen. Changes in chloroplast ultrastructure in non-symptomatic leaf areas showing different NPQ levels were also investigated. A gradient of ultrastructural modifications was observed among the different areas.

Keywords Biotic stress · Chlorophyll fluorescence imaging · Non-photochemical quenching · Pepper mild mottle virus · Photosystem II · Tobamovirus

Abbreviations

AS	asymptomatic leaf
C	chloroplast
CCD	charge coupled device
Chl *a*	chlorophyll a
Chl-FI	chlorophyll fluorescence imaging
CP	viral coat protein
CW	cell wall
dpi	days post-infection
F	actual fluorescence
F'_M	maximum fluorescence in the light-adapted state
F_M	maximal fluorescence in the dark-adapted state
G	*grana*
L	Sharp and narrow band marking the border between leaf areas with different NPQ values in NPQ_{30} images from AS leaves.
La	stroma *lamellae*
LHCII	light harvesting complex II
Mt	mitochondrion
M	outer region of the mesophyll in AS leaves
NPQ	non-photochemical quenching

The paper is dedicated to the memory of Prof. Dr López Gorgé (1935–2004)

M. L. Pérez-Bueno · I. García-Luque
Plant Biology Department, Centro Investigaciones Biológicas, CSIC, Ramiro de Maeztu 9, Madrid 28040, Spain

M. Ciscato · M. vandeVen · R. Valcke
Dept. SBG, Centre for Environmental Sciences, Laboratory of Molecular and Physical Plant Physiology, Hasselt University, Agoralaan, Bldg. D, Diepenbeek B-3590, Belgium

M. Barón (✉) · M. L. Pérez-Bueno
Estación Experimental del Zaidín, CSIC, Profesor Albareda 1, Granada 18008, Spain
e-mail: mbaron@eez.csic.es

NPQ_t	non-photochemical quenching at referred kinetics time, *t*
OEC	oxygen-evolving complex
PAR	photosynthetically active radiation
Pg	*plastoglobuli*
Pm	plasmatic membrane
PMMoV-I	pepper mild mottle virus Italian strain
PSI	photosystem I
PSII	photosystem II
PVX	potato virus X
ROI	region of interest
S	starch grains
TMV	tobacco mosaic virus
V	areas surrounding the main veins in AS leaves
Va	vacuole
VP	virus particles

Introduction

Viruses induce in their hosts a wide range of foliar visual symptoms with a heterogeneous distribution (mottle, mosaic, chlorosis, necrosis, etc). In some host–virus systems, the metabolic heterogeneity of the infected leaves regarding to local changes in CO_2 assimilation, photosynthetic efficiency, starch accumulation and chlorophyll a (Chl *a*) fluorescence have been documented (Técsi et al. 1996; Chou et al. 2000; Havelda and Maule 2000).

The development of imaging techniques to monitor the red fluorescence emitted by Chl *a*, so called fluorescence imaging (Chl-FI) systems, has allowed the study of the spatial and temporal heterogeneity of the foliar photosynthetic efficiency in response to different biotic and abiotic stress factors (Daley et al. 1989; Fenton and Crofts 1990; Genty and Meyer 1994; Técsi et al. 1994; Ning et al. 1995; Rolfe and Scholes 1995; Lichtenthaler 1996; Lichtenthaler et al. 1997; Oxborough and Baker 1997; Leipner et al. 2001; Fryer et al. 2002; Lawson et al. 2002).

This Chl-FI tool is especially valuable in the case of biotic stress where no uniform alteration of the foliar metabolism, neither of the photosynthetic activity nor the symptom development is expected.

Since the pioneering study in which Björn and Forsberg (1979) applied imaging of chlorophyll luminescence to reveal non-uniform leaf photosynthesis in response to pathogens, the development of further Chl-FI prototypes have provided valuable tools to follow the infection and investigate its effect on the photosynthetic machinery. Thus, it is now documented for some plant–pathogen interactions that photosynthesis is severely unpaired in the symptomatic areas from either fungal- or viral-infected plants, as deduced from Chl-FI (Esfeld et al. 1995; Scholes and Rolfe 1996; Osmond et al. 1998; Chou et al. 2000; Lohaus et al. 2000). In fungal infections, it has been described that the rate of photosynthetic inhibition is associated with the severity of the symptoms. It has also been shown that changes in some fluorescence parameters precede the symptom development (Ning et al. 1995; Peterson and Aylor 1995; Soukupová et al. 2003).

In addition, the analysis of the data obtained by Chl-FI could be indicative of the underlying metabolic changes in the infected plants. Thus, the local changes in photochemical and non-photochemical quenchings have been associated to alterations of the Benson–Calvin cycle capacity and changes in the carbohydrate metabolism (Esfeld et al. 1995; Rolfe and Scholes 1995; Scholes and Rolfe 1996; Chou et al. 2000). Changes in stomatal conductance and metabolic inhibition of photosynthesis have also been reported (Meyer et al. 2001).

In virus-infected plants, Balachandran and Osmond (1994) and Balachandran et al. (1994) used Chl-FI to diagnose early stages of *Nicotiana tabacum* infection by tobacco mosaic virus (TMV). In these studies, it was shown that the earliest in vivo sign of infection is a reduction of fluorescence yield, prior to enhancement of unquenched fluorescence and light-dependent development of chlorotic mosaic symptoms following photoinhibitory damage. As for fungal infection, Osmond et al. (1998) and Lohaus et al. (2000) showed in *Abutilon* mosaic virus-infected *Abutilon striatum* leaves that the impaired non-photochemical quenching (NPQ) in the infected tissues reflects the state of symptom development.

According to Balachandran et al. (1997), early responses of the photosynthetic parameters to pathogen infection suggest that photoprotective as well as photoinhibitory processes contributed to local damage of the photosynthetic apparatus and symptom development.

By combining both Chl-FI and thermography analysis, Chaerle et al. (2004) were able to distinguish the early stages of a plant–virus interaction from a plant-fungus one, proposing that *disease signatures* of different plant–pathogen interactions could facilitate a pre-symptomatic diagnosis.

In the present work, Chl-FI was used to study a compatible host–pathogen interaction, *Nicotiana benthamiana* plants infected by the Italian strain of the pepper mild mottle virus (PMMoV-I). In previous studies

(Barón et al. 1995; Rahoutei et al. 1998, 1999, 2000; Pérez-Bueno et al. 2004), we have analysed the effect of infection with the Spanish and Italian strains of PMMoV upon photosynthesis in these plants. We have shown in infected plants that, photosystem II (PSII) electron transport is inhibited due to changes in the protein composition of the oxygen-evolving complex (OEC) in the thylakoid membranes. In addition, point measurements of modulated Chl-fluorescence demonstrated that NPQ increases during the symptom development.

The Chl-FI system (Valcke et al. 1999; Ciscato 2000) used in this study allows gaining further insight into the processes induced by tobamovirus infection in the photosynthetic apparatus.

Leaf photosynthesis was mapped and images of different fluorescence parameters were obtained at different points of the fluorescence induction curve, as well as at different post-infection times, to investigate which one could better discriminate control from infected leaves in the absence of symptoms.

Kinetic Chl-FI revealed a complex and heterogeneous time-varying spatial pattern of the photosynthetic efficiency and non-photochemical processes during pathogenesis. To test whether the heterogeneity of the photosynthetic pattern (Chl-FI images) found in the asymptomatic (AS) leaves from infected plants could be associated to the pathogen distribution, tissue-prints for pathogen detection were carried out. Ultrastructural studies of chloroplasts from infected plants were also addressed, to test whether the decreased capacity of photosynthesis and changes in the Chl-FI parameters could be associated to modifications in chloroplast structure.

To our knowledge, this is the first study of infected plants where the whole quenching analysis was carried out by mean of Chl-FI from the early to the later infection stages of the host-plant. We were able to obtain images of NPQ (other parameters are not shown) at different points of the fluorescence induction curve; some of them (NPQ_{20}, NPQ_{30}, NPQ_{300}) could be used as stress indicators. In addition, we have demonstrated a correlation between changes in the chlorophyll fluorescence parameter NPQ and the location of the virus, as well as the chloroplast ultrastructure in asymptomatic leaves.

Material and methods

Plant and virus material

N. benthamiana Gray plants were cultivated in a growth chamber at 200 μmol m^{-2} s^{-1} PAR (photosynthetically active radiation), generated by a combination of Sylvania (Danvers, MA, USA) VHO cool white fluorescent and incandescent lamps, with a 16/8 h photoperiod, a temperature regime of 25°C/20°C (day/night) and a relative humidity of 80%.

Three lower leaves of plants at the 4–5 fully expanded leaves stage were inoculated. Carborundum-dusted leaves were mechanically inoculated with 50 μl of *inocula* per leaf (50 μg of virus per ml of 20 mM sodium phosphate/biphosphate buffer pH 7.0) by gently rubbing of the leaf surface. Visual symptoms start to show at 5–7 days post-infection (dpi). Leaves developed after inoculation (symptomatic leaves) showed a severe wrinkling and curling; in contrast, no symptoms were observed in the three inoculated leaves and neither in those upper fully expanded leaves that were not inoculated. These non-inoculated leaves will be referred as asymptomatic leaves (Rahoutei et al. 2000). After 14 dpi, stunting of the plant was clearly evident. Summarizing, we can distinguish three kinds of leaves in the infected plants: inoculated, asymptomatic and symptomatic; only the asymptomatic ones were used for the experiments.

The origin of the Italian strain of PMMoV has previously been reported (Wetter et al. 1984).

Red fluorescence imaging by the saturation pulse mode

The completely computer-controlled Chl-FI system used in this work (Valcke et al. 1999; Ciscato 2000) consists of excitation, imaging and control units. A large area of cold illumination ($\lambda < 650$ nm) is provided at two intensity levels by eight fibre bundles mounted in a circular pattern. Actinic light (220 μE m^{-2} s^{-1}) is provided by a blue-filtered 150 W xenon lamp, model FOT 150 FiberOptic (P. + P. AG, Spreitenbach, Switzerland) and saturating light (1200 μE m^{-2} s^{-1}) provided by four additional 250 W xenon-lamps (Osram Xenophot HLX, Osram GmbH, München, Germany) placed in LQ 2600 lamp houses (Fiberoptic-Heim AG, Uetikon am See, Switzerland) fitted with saturated $CuSO_4$ solution as blue low-pass filters.

Fluorescence is collected via a model XC-75 (Sony Corporation, Tokyo, Japan) black & white CCD (charge-coupled device) camera fitted with zoom lens and a red high-pass filter ($\lambda > 680$ nm) model B + W 092 (Schneider Optics Inc., Hauppage, NY, USA), corresponding to Schott RG 695 (Valcke et al. 1999). Operated in its linear range the camera signal is digitised with an Osprey-100 frame grabber card, (Osprey Technologies, Inc., Morrisville NC, USA) and an AD/DA converter board (PCL-711B, Advantech Co., Ltd.,

Sunnyvale CA, USA), both placed in a Dell Dimension XPS R450, Dell Computer Corporation, Round Rock TX, USA).

Instrument control and data collection is carried out under Linux, distribution Slackware 7.0, Kernel version 2.0.13, for its robustness and ample freeware availability. Software for recording and processing the images is described in Ciscato (2000). Raw 32-bit images are collected typically for a 640×480 pixel frame size. This corresponds with an 8.5×6.4 cm area. Image processing was done via scripts for the (free) student version of the KhorosPro2001 suite (Khoral Research Inc., Albuquerque NM, USA). Results from dark signal subtraction, illumination correction, center region-of-interest (ROI) selection and basic statistical histogram analysis are stored in SA (Scientific American) false colour (Khoros) or in grey scale as 8-bit ASCII files for further processing.

Plants were first dark-adapted for 1 h before the start of the measurements. For quenching analysis, attached AS leaves were illuminated with continuous blue actinic light (200 μE m^{-2} s^{-1}) and saturating pulses (1200 μE m^{-2} s^{-1}) at 2, 5, 10, 20, 30, 60, 90, 120, 180, 240 and 300 s. Previously to the Chl-FI experiments, we have carried out measurements by the PEA fluorometer to decide the intensity of saturation light pulse.

These measurements allow us to follow the fluorescence quenching induction as well as the analysis of quenching levels in the steady state of photosynthesis, which is considered to be reached at 300 s. Images were captured during the application of the first saturating pulse of light (maximal fluorescence in the dark-adapted state, F_M), 1 s before (actual fluorescence, F) and during every pulse (maximum fluorescence in the light-adapted state, F'_M). From the processed images, the parameter NPQ ($F_M/F'_M - 1$) was calculated by computing pixel by pixel. Four different experiments with five controls and virus-infected plants were carried out.

As an additional step in the image analysis and in order to reduce the influence of varying surface properties, four ROIs of 10×10 pixels were selected in all series of images taken from control and asymptomatic leaves to follow the time course of fluorescence quenching. Mean values are obtained from the analysis of three different leaves.

The ImageJ software package (rsb.info.nih.gov/ij) was used to obtain fluorescence profiles along a 451 pixel line drawn in the middle of the leaf, and centred on the midrib.

Tissue print

Localization of viral coat protein (CP) in leaves was performed by tissue print analysis using specific antiserum against PMMoV-I CP (Alonso et al. 1989). Non-specific binding was reduced by pre-absorbing the immune antiserum with acetone powder obtained from stems and leaves of young healthy *N. benthamiana* plants (Ruiz del Pino et al. 2003). Whole leaves from healthy and infected plants were imprinted on nitrocellulose sheets and assayed as previously described (Maliga et al. 1995). Membranes were incubated with the PMMoV-CP specific antiserum at the appropriate dilutions and then incubated with goat anti-rabbit alkaline phosphatase-IgG. Bound antibodies were detected using nitro-blue tetrazolium/5-bromo-4-chloro-3-indolyl phosphate (NBT/BCIP, Bio-Rad).

Electron microscopy

For electron microscopy analysis, samples from healthy and infected leaves were collected and fixed overnight at 4°C in 2.5% glutaraldehyde and 0.1% malachite green (w/v) buffered in 50 mM Na-PIPES pH 7.5. Samples were washed three times in 50 mM Na-PIPES pH 7.5 and post-fixed for 3 h at room temperature in 2% osmium tetroxide in 0.2 M sodium cacodylate. The tissue pieces were then rinsed in cacodylate buffer, dehydrated in ethanol series and embedded in ERL 4206 Spurr resin (Fluka, Buchs, Switzerland) after incubation in propylene oxide 100% for 1 h. Ultrathin sections were cut on a Leica ultracut ultramicrotome, stained in a solution of uranyl acetate and lead citrate. Later on the cuts were examined under a Philips 208S electron microscope equipped with a Kodak Megaplus Camera model 16.1.

Results

Viral infection induces temporal and spatial variations in the photosynthetic efficiency and non-photochemical processes

The kinetic of pathogenesis in *N. benthamiana* infected by PMMoV-I was followed by capturing images of different Chl-FI parameters from healthy and infected plants. During the first post-infection week, images of Chl-FI parameters were daily collected and then at 7, 10, 14, 17, 21, 24 and 28 dpi. AS leaves and their equivalent leaves from healthy plants were analysed. The observed changes were quite complex and a large

amount of information was obtained as a function of the post-infection time and selected imaged parameters. Out of the different parameters analysed, it was found that NPQ maximized the differences between healthy and infected plants. Therefore, only a small part of the information is displayed in the following figures.

During the first 7 days after inoculation no difference in Chl-FI images was found between AS leaves from virus-infected and healthy plants. The first changes were observed at the middle stage of studied period infection, 14–17 dpi. Maximum differences were observed in the NPQ pictures (Fig. 1).

Figure 1a, b display the NPQ kinetics during the fluorescence transient measured in leaves of healthy plants and AS leaves of PMMoV-I infected plants at 17 dpi, respectively. They show a complex, time-varying spatial pattern of non-photochemical quenching processes in the infected plants. Chl-FI reveals a large contrast between the NPQ images from AS leaves and corresponding control leaves from 20 s of the onset illumination. In NPQ_{20} and NPQ_{30} images (after 20 and 30 s illumination) from infected AS leaves, three well-defined areas are displayed. A sharp and narrow dark blue band showing the lowest NPQ value marks the border between the area corresponding to the midrib and midrib branching veins (class I and II veins; see *N. benthamiana* vein classification in Roberts et al. 1997) and the rest of the leaf blade. The NPQ value at 300 s (NPQ_{300}) exhibits a dramatic increase in that vein area of AS leaves, whereas it remains unaffected in the rest of the leaf.

NPQ images of the corresponding leaves in control plants display a completely different spatial pattern in most of the kinetics points (20–300 s). NPQ increases up to 30 s and diminishes to reach a relative minimum at 90–120 s corresponding to the second maximum in the fluorescence induction reflecting the activation of Benson–Calvin cycle, after which the terminal steady-state is reached (300 s of illumination). NPQ_{300} values are much lower in control leaves than those in asymptomatic ones and no defined NPQ pattern is found in the corresponding images, in contrast with that described for infected leaves.

In accordance with the previous data, we have chosen two time points in the NPQ kinetics during the fluorescence transient, where the contrast between healthy and infected plants is high enough to show the heterogeneity of the photosynthetic processes in virus-infected leaves: NPQ_{30} after 30 s illumination during the fluorescence induction (NPQ_{30}; Fig. 1c, d) and after 300 s (NPQ_{300}; Fig. 1e, f). Images were collected from healthy and AS leaves from infected plants at different post-inoculation time 7, 14, 17, 21, 24 and 28 dpi.

In the images corresponding to NPQ_{30}, the control leaves (Fig. 1c) do not show any distinctive spatial pattern, compared to those infected leaves (Fig. 1d). At 14 dpi the main veins of the AS leaf have developed lower NPQ values than the rest of the leaf surface. After 17 dpi the three NPQ areas already mentioned were evident. The low value of NPQ_{30} displayed in the images from infected leaves in the final infection stages (24–28 dpi) represent an impaired fluorescence quenching, which could be attributed to dramatic changes in the thylakoid membrane and PSII function.

Analysing NPQ, changes in NPQ_{300} during the pathogenesis are more impressive (Fig. 1e, f). After 14 dpi the areas surrounding the main veins (class I and II) of the AS leaf showed a slight increase in NPQ values; but, 3 days later (17 dpi) this parameter was amplified dramatically in the vein area. Afterwards, at 21–24 dpi, the whole AS leaf showed a very high NPQ quite homogeneous over the whole leaf. Meanwhile the corresponding leaves from healthy plants show a lower NPQ over the leaf surface from 7 to 24 dpi. In the final infection steps, when senescence is predominant, both healthy and infected leaves show a low NPQ.

NPQ_{300} profiles across the leaf surface of both AS leaves from infected plants and their corresponding controls were plotted at 17 and 21 dpi, to visualise the evolution of the NPQ differences between veins and surrounding tissues (Fig. 2a, b). They illustrate a greater spatial heterogeneity of the non-photochemical process pattern from infected plants compared with the controls.

In addition, NPQ time-course has been followed in AS leaves at 17 dpi in the three areas with different NPQ levels, visible in the corresponding images from 20–30 s (Fig. 3, NPQ_{30} s). Random ROIs were selected in the areas surrounding the midrib and secondary veins (V), a long narrow lane (L), and from this one the outer region of the mesophyll (M). The area L showed the lowest NPQ values from 20 s during the fluorescence induction (Fig. 3 insert b, see also Fig. 1). These kinetics were compared with those from healthy plants measured in equivalent V and M areas of the leaf (Fig. 3 insert a). In the control leaves both areas showed similar NPQ kinetics. In contrast, in leaves from infected plants the three mentioned areas corresponded to areas showing strikingly different levels of non-photochemical energy dissipation, the highest one directly surrounding the veins.

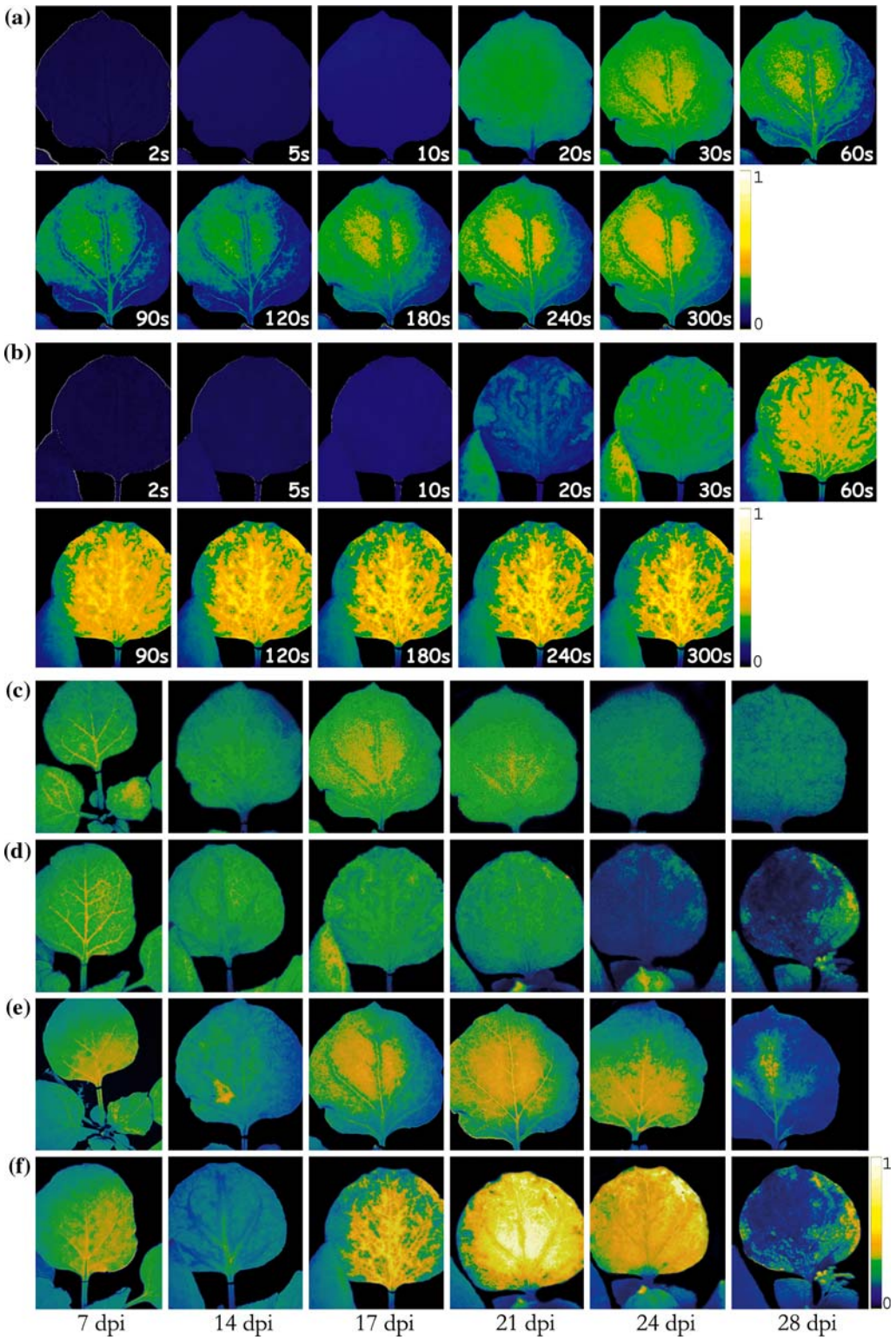

Fig. 1 Images of non-photochemical quenching kinetics at 17 dpi from healthy and PMMoV-I infected plants: kinetics during fluorescence induction from healthy (**a**) and asymptomatic leaves from infected plants (**b**) at 17 dpi. NPQ_{30} images at different dpi from healthy (**c**) and asymptomatic leaves of infected plants (**d**). Images of non photochemical quenching at NPQ_{300} from healthy (**e**) and asymptomatic leaves of PMMoV-I infected plants (**f**) during pathogenesis. The colour scale bar indicates the NPQ intensity of the leaf pixels given in false colours from high (white) to low (blue) values

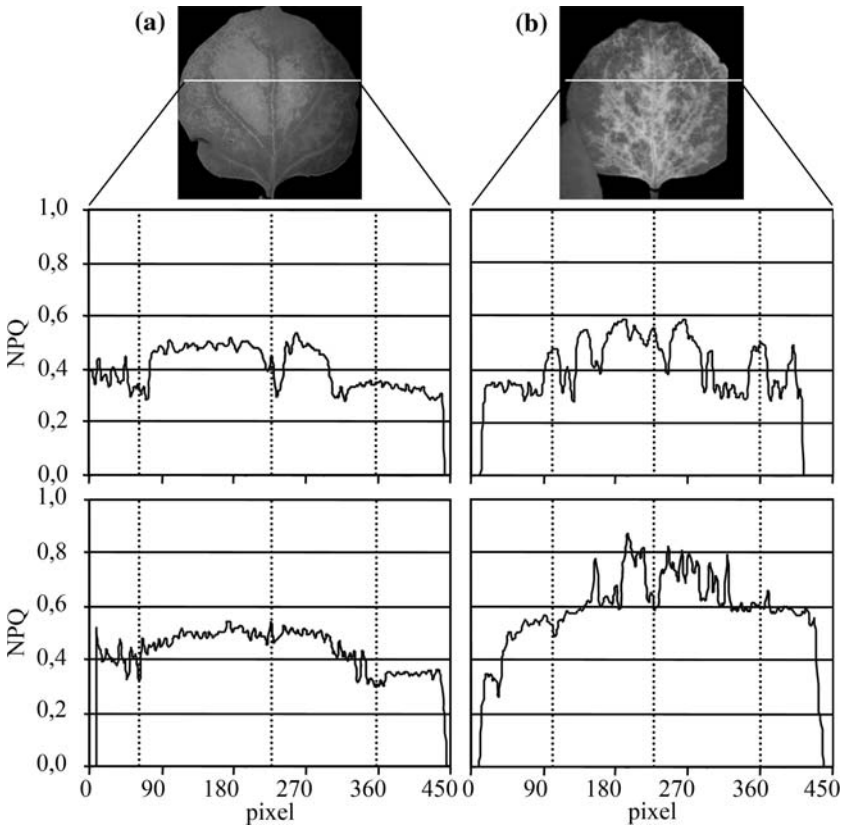

Fig. 2 NPQ local changes during infection (17 and 21 dpi) in leaf tissues adjacent to major veins. NPQ profiles are shown along a 451 pixel line drawn in the middle of the leaf, and centred on the midrib. The NPQ images shown correspond to 17 dpi. Control plants (**a**), PMMoV-I-infected plants (**b**)

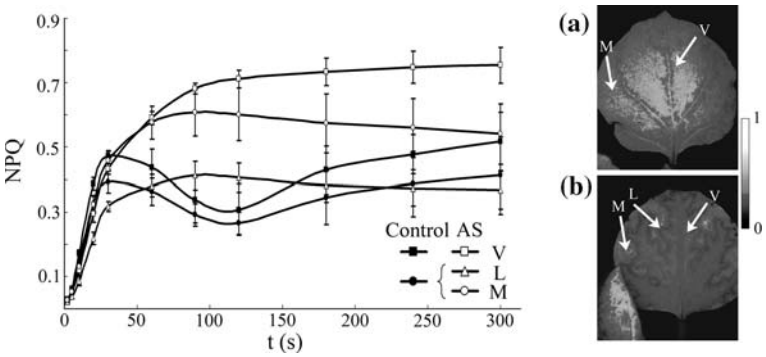

Fig. 3 Non-photochemical quenching time-course measured in different regions of interest from control healthy and asymptomatic leaves of infected plants at 17 dpi. Insert: defined areas in NPQ_{30} images from healthy (**a**) and asymptomatic leaves from PMMoV-I infected plants (**b**) leaves. The scale bar indicates the NPQ intensity of the leaf pixels

Differences in NPQ values within the infected leaf are correlated to viral accumulation detected by tissue print and electron microscopy

We have described three different areas, attending to their NPQ kinetics, in AS leaves from infected plants at 17 dpi. Next, we wanted to test whether the heterogeneity of the NPQ pattern found in these leaves could be related to viral distribution. Therefore, AS leaves from both control and PMMoV-I infected plants were collected at 7, 14, 17, 21 and 28 dpi, blotted onto nitrocellulose and probed for the presence of viral CP using a specific PMMoV-CP antiserum.

As shown in Fig. 4, the viral CP was first detected in the AS leaves at 21 and 28 dpi, albeit its distribution changed during the infection. Earlier, at 17 dpi, only a weak reaction was detected in the leaf base close to the petiole (data not shown). Initially, the reaction signal was detected in areas close to the main veins at 21 dpi, indicating that viral accumulation was essentially associated to these regions. Later on, at 28 dpi, viral CP could be detected all over the leaf, indicating that viral infection had spread through the leaf.

In order to know whether different NPQ levels across the infected leaves were associated with ultrastructural changes in the chloroplast, electron

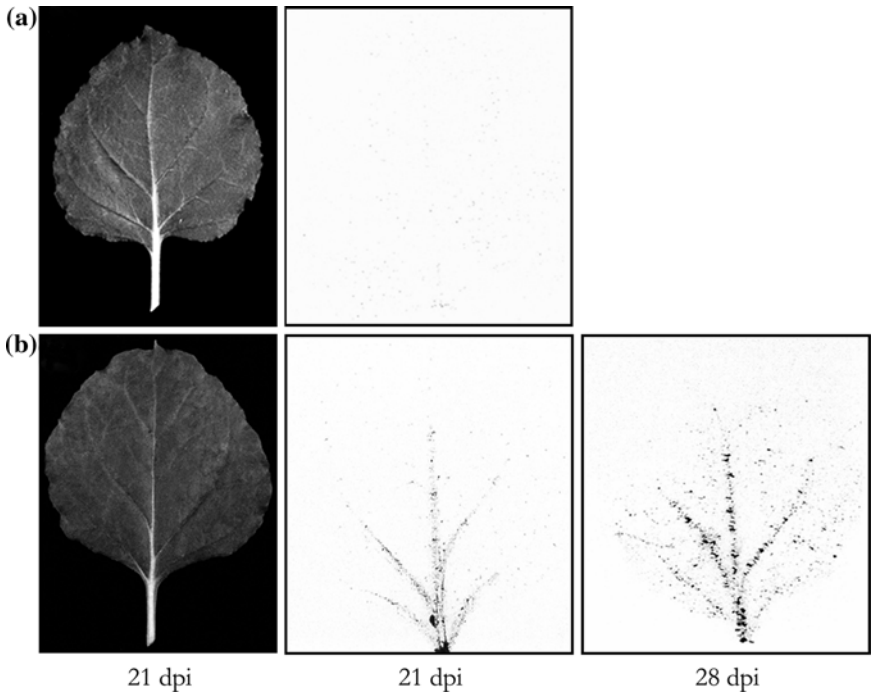

Fig. 4 Tissue prints using the antibody against the viral coat protein at different post-infection times from healthy (**a**) and asymptomatic leaves from PMMoV-I infected plants (**b**). Left panels: Reflectance pictures of the corresponding leaves

micrographs from control and AS leaves were taken at 17 dpi. Samples were collected from the three different areas (V, L and M) defined in the corresponding NPQ_{20} images (Fig. 3 insert b). Chloroplast structure in these regions were compared to the equivalent regions from healthy leaves, where only two zones were considered, V and M (Fig. 3 insert a).

Transmission electron micrographs of chloroplasts from the V and M areas in control leaves (Fig. 5a and b, respectively) exhibited the typical ellipsoidal shape, well-developed thylakoid membranes and *grana* stacking. In chloroplasts from both areas of control leaves only, non-opaque *plastoglobuli* were detected.

Chloroplasts from the V area in infected leaves (Fig. 5c, d) were deformed, swollen, and contained large starch grains of irregular shape, which apparently causes the displacement of the *grana* to the edge of the organelle. In addition, two types of *plastoglobuli*, osmiophilic and those of less electron opacity could be observed in these cells (Fig. 5c). Typical tobamovirus particles were also visualized dispersed in the cytoplasm (Fig. 5d).

In the L area from the infected leaves (Fig. 5e, f), the chloroplast ultrastructures were similar to those from the V area: globular plastids with large and irregular starch grains which displaced the granal structure. The thylakoid organization was loosened, although some *grana* remained intact. Virions were also detected in the cytoplasm (Fig. 5f).

In the M area from AS leaves, the chloroplast contained large but regular starch grains, albeit showing reduced with respect to those observed in the V and L areas. Part of the thylakoid structure remains intact. Osmiophilic and less opaque *plastoglobuli* were also present in these samples. In contrast to the V and L areas, no viral particles could be detected in cells of M area in any of the analysed fields (Fig. 5g, h).

Discussion

Fluorescence imaging

The development of FI systems was a valuable contribution to the study of the effect of biotic stress in plants, due to the physiological and morphological heterogeneity of the pathogen-infected leaf (Balachandran et al. 1994; Esfeld et al. 1995; Peterson and Aylor 1995; Scholes and Rolfe 1996; Osmond et al. 1998; Chou et al. 2000; Lohaus et al. 2000; Meyer et al. 2001; Soukupová et al. 2003; Chaerle et al. 2004).

The present work, to our knowledge, is the first one to show that non-photochemical quenching of a whole leaf has been analysed *in planta* using Chl-FI and correlated with the location of a virus by inmunolocalization and changes in chloroplast ultrastructure using electron microscopy. According to our results, NPQ seems to be the most adequate Chl fluorescence parameter to assess the effect of tobamoviral infection

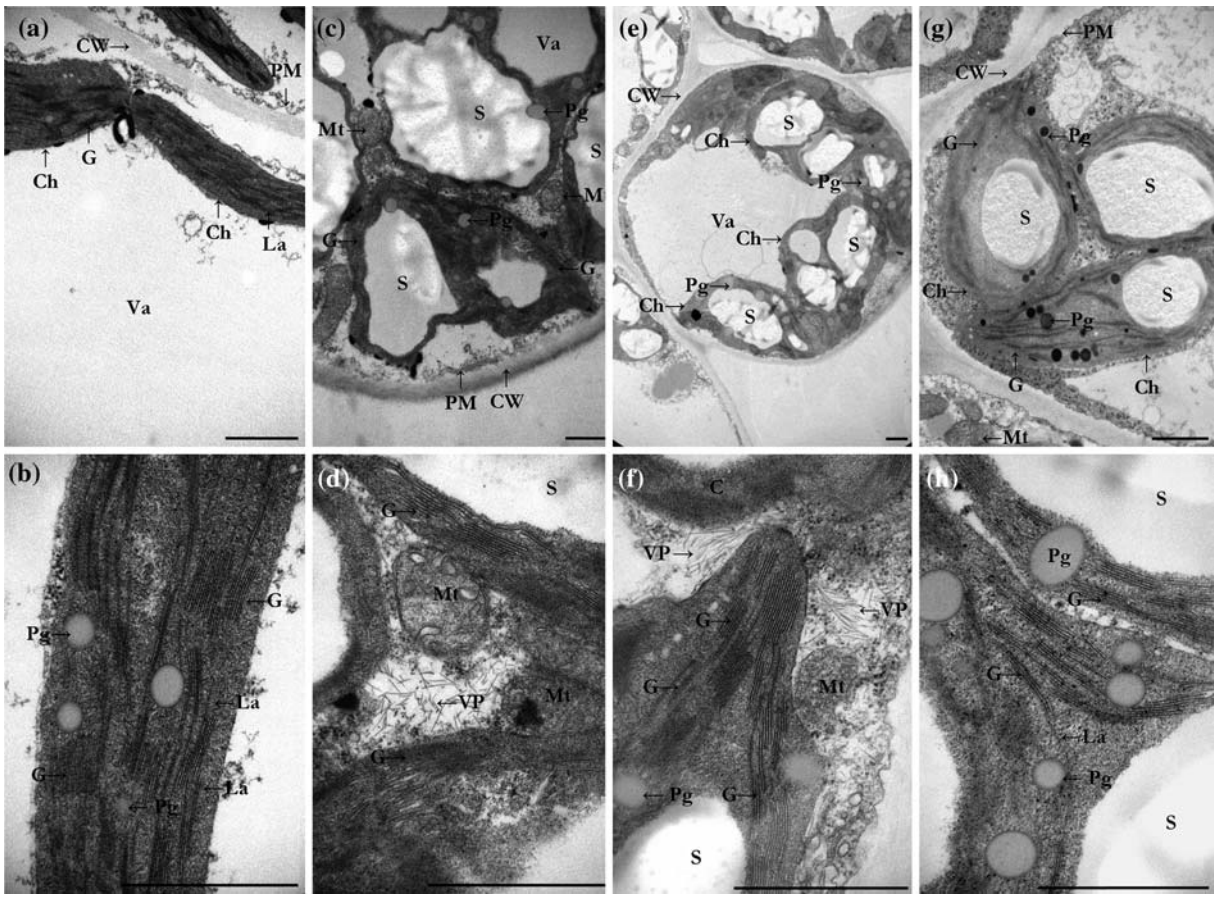

Fig. 5 Transmission electron micrographs of *N. benthamiana* cells and chloroplasts from the V (**a**) and M (**b**) regions of control leaves, as well as from the V area in asymptomatic leaves of PMMoV-I infected plants at 17 dpi (**c** and **d**). Extension Fig. 5: Chloroplasts from infected plants at the same post-infection time in areas L (**e**, **f**) and M (**g**, **h**) of asymptomatic leaves. Scale, 1 μm; C, chloroplast; CW, cell wall; La, stroma *lamellae*; G, *grana*; M, mithochondrion; Pg, *plastoglobuli*; Pm, plasmatic membrane; S, starch grains; VP, virus particles; Va, vacuole

on the chloroplast, providing the highest contrast between the infected and non-infected plants, in leaves not showing any symptoms. Other fluorescence parameter such as the quantum yield of PSII were also measured (data not shown), but they did not demonstrate to be useful for stress detection during the infection process. The data presented here are well in accordance with those from Osmond et al. (1998) and Lohaus et al. (2000), and expand them to the asymptomatic areas of the plant. Asymptomatic leaves of PMMoV-I infected plants display a complex and characteristic NPQ kinetics patterns, depending upon the infection stage.

Earlier work by Rahoutei et al. (2000) demonstrated that chlorophyll content was not significantly different between the leaves from infected and control plants. Thus, other factors are responsible for the observed fluorescence changes in PMMoV-infected plants.

In the AS leaf, NPQ values are low around the invasion front, indicative of high photosynthetic rates. In the areas already invaded by the pathogen high NPQ values are detected, thus the leaf area with higher NPQ values increases during the infection time. At the latest stages of infection, the leaf displays the lowest NPQ values, denoting that senescence is predominant and photochemical as well as non-photochemical processes are totally down-regulated.

Viral-induced changes on the NPQ leaf pattern are visible earlier (14 dpi) than viral elements could be detected by either tissue print (for the CP, at 17–21 dpi) or Northern blot for the viral RNA (21 dpi; Pérez-Bueno 2003).

Likewise, viral distribution within the leaf changed during the infection process. At the earliest time point in which the pattern of viral distribution was detected, it was found essentially to be associated with the area

surrounding major veins (class I and II). Later on, it was detected all over the leaf (Fig. 4). This distribution pattern is well correlated with the pattern previously established for the systemic invasion of *N. benthamiana* plants by TMV and potato virus X (PVX) as well as for other RNA viruses, i.e. virus discharge from phloem-associated cells in major veins and further invasion of the entire leaf (Roberts et al. 1997; Cheng et al. 2000; rev. Hull 2002).

The correlation found between NPQ amplification and virus localization strongly supports that the increase in the local NPQ values is associated with the areas invaded by the pathogen. In *Arabidopsis thaliana* plants infected by the fungus *Albugo candida* it was found that local NPQ increase precedes the symptom appearance in the same areas (Chou et al. 2000). Berger and associates (2004) showed in *Lycopersicum esculentum* plants infected by either bacteria or fungus, that NPQ changes were confined to the direct vicinity of the infected area, whereas photosynthesis remains unaffected in the non-invaded areas of the leaf. These findings suggest that changes in NPQ values in the regions colonized by the pathogen are a relevant phenomenon in plant pathogenesis.

On the other hand, the lower NPQ values detected in the leaf area L at the middle stage of infection suggest an increase in photosynthetic activity in the area. In strong accordance with previous work carried out with *Cucurbita pepo* cotyledons infected with Cucumber mosaic virus (Técsi et al. 1994, 1996) and *L. esculentum* infected by *P. syringae*, *X. campestri* and *B. cinerea* (Berger et al. 2004), the data here presented indicate that this area may correspond to the edge of the infection, since its position changes within the leaf throughout the time, and its pattern is similar to that found for viral coat protein at the earliest time in which it is detected. Whether this area corresponds to the infection front, where viral replication is very active, and/or the cells located ahead of the infection front, at present remains unknown. In any case, it is plausible to consider that an increase in photosynthetic activity at the boundary of the viral infection front could be required not only to support the synthesis of viral products, but also to mount the host responses that could restore the cell damage inflicted by the pathogen, as well as to limit viral replication, accumulation or spread (Técsi et al. 1996; Havelda and Maule 2000; rev. Karpinski et al. 2003; Berger et al. 2004).

In accordance with Osmond et al. (1998) and Chou et al. (2000), we have found in previous work with *N. benthamiana* plants infected with PMMoV-I, decreased levels of the mRNA coding the small Rubisco subunit and the light harvesting complex II (LHCII), respectively (Pérez-Bueno 2003). Thus, virus-induced disturbances of the Benson–Calvin cycle could lead to an increase of the intrathylakoidal pH gradient (Ruban and Horton 1995), contributing to the remarkable NPQ development during infection. Analysis at 17 dpi of NPQ kinetics in different areas of AS leaves defined according to NPQ values (V, L, M; Fig. 3) confirms this assumption. During the fluorescence induction no NPQ relaxation phase was found in any of these areas from infected leaves. In contrast, control leaves display an increase in NPQ values during the first seconds followed by a decline, related to Benson–Calvin cycle activation.

In addition, our preliminary analysis (Sajnani et al. 2005) of *N. benthamiana* leaves infected with PMMoV-I by thermoluminescence, indicate that cyclic electron transport around PSI (Peltier and Cournac 2002) could be stimulated during viral infection; according to Horton et al. (2005) this can modulate the pH gradient and consequently NPQ processes. Electron consuming pathways involving cyclic electron transport are considered useful photoprotective mechanisms (Karpinski et al. 2003).

Moreover, our previous studies (Rahoutei et al. 1998, 1999, 2000; Pérez-Bueno et al. 2004) revealed damage to the PSII donor site due to a decrease in its extrinsic protein levels in virus-infected plants. Thus, PSII centers of virus-infected plants show similarities with the *dissipative* PSII centers described by other authors (van Wijk et al. 1993; Critchley and Russell 1994). These dissipative centers lack OEC proteins and associated cofactors; they do not participate in linear electron transport and could be involved in alternative electron pathways, down-regulating PSII and protecting other centers that are fully functional.

The increase in NPQ during the viral infection is a host defence response that could delay photoinhibition until the final infection steps (Wright et al. 1995a, b; Balachandran et al. 1997). In fact, we have previously shown that only at 21 dpi, photoinhibition occurs with a decrease in F_V/F_M ratio (Rahoutei et al. 2000; fluorescence point measurements); at this stage, we have also found by the HTL (high temperature thermoluminescence analysis), oxidative damage in thylakoid membranes isolated from infected plants (Rahoutei et al. 1999).

Summarizing, different processes contribute to the enhancement of energy dissipation in the chloroplast of PMMoV-I-infected plants: The existence of some OEC-depleted dissipative PSII centers, disturbances on Benson–Calvin cycle and functional PSI cycle that could provide ATP for the pathogen replication and defence mechanisms.

However, the goal of this paper is not to identify the NPQ origin, but to locate a fluorescence signal allowing the differentiation between healthy and infected plants and correlate it with the pathogen spreading.

The spatial similarity found between viral invasion and NPQ image seems to be very promising for the study of metabolic changes and transport pathways during pathogen infection. Mapping the appropriate Chl-FI parameter to follow pathogenesis, NPQ in the case of PMMoV-I infection, will provide *disease signatures* for different plant–pathogen interactions and will allow pathogen detection in the absence of symptoms (Chaerle and van der Straeten 2001; Baker and Rosenqvist 2004; Chaerle et al. 2004).

Ultrastructural analysis

A gradient of ultrastructural modifications was observed among the three different areas defined by their NPQ values. Chloroplasts of the areas V and L showed distinct ultrastructural changes associated with viral content, whereas changes in the M area could be related to systemic signalling from invaded tissues of the neighbouring area. The changes observed in the PMMoV-I infected *N. benthamiana* cells from AS leaves—occurrence of large and irregular starch grains in the swollen and deformed plastids, accumulation of osmiophilic plastoglobuli and disorganization of chloroplast lamellar structures—are similar to those previously detected in TMV-infected cucumber cotyledons (Cohen and Loebenstein 1974), where the infection is restricted to the inoculated leaves forming starch lesions (Lindner et al. 1959). Thus, these data suggest that some changes in host responses to avirulent or virulent pathogens could be similar.

The observed increase in starch content within chloroplasts, as we report here, has been associated with different plant–pathogen interactions as well as to some abiotic stress conditions (Esau and Cronshaw 1967; Goodmann et al. 1986; Hull 2002). Different metabolic processes, such as alterations in the Benson–Calvin cycle, modifications in the permeability of chloroplast membranes and disturbances on the source–sink relationship were found to be correlated with this phenomenon (Wright et al. 1995a, b; Ouzounidou et al. 1997; Hull 2002), but the precise mechanism(s) responsible remain unknown. From Holmes (1931) pioneering work, it is known that TMV infections interfere with starch mobilization, reducing both the rates of accumulation and degradation. Taking into account the complexity of starch turnover within the plant (rev. Beck and Ziegler 1989; Ball and Morell 2003; Zeeman et al. 2004), its higher accumulation in stressed plants could be due to a severe impairment between the rates of starch breakdown and its biosynthesis, which in turn could reflect the profound metabolic alterations suffered by the host as a consequence of pathogen invasion.

On the other hand, the abundance of *plastoglobuli* and disorganization of chloroplast lamellar structures resemble those of chloroplasts from senescent leaves (Almási et al. 1996, 2001 and references therein; del Río et al. 1998). Lehto et al. (2003) assign the chloroplast malformations in tobacco plants infected with the flavum strain of TMV to deficient synthesis and assembly of thylakoid proteins. In this sense, we have previously demonstrated disturbances of OEC synthesis during early infection stages in PMMoV-infected *N. benthamiana* plants (Rahoutei et al. 2000; Pérez-Bueno 2003; Pérez-Bueno et al. 2004). The formation of *plastoglobuli* is thought to be linked to the breakdown of thylakoids that accompanies senescence (del Río et al. 1998). Thylakoid membrane degradation by lipid peroxidation has been shown to take place at the final infection steps (Rahoutei et al. 1999). Therefore, the low NPQ values displayed in the NPQ_{30} and NPQ_{300} images from AS leaves in the final infection stages represent an impaired fluorescence quenching, which could be attributed to dramatic changes in the thylakoid membrane and PSII function. These virus-induced changes in the thylakoid membranes and photosynthetic complexes could to some extent be responsible for the chloroplast malformations found in AS leaves of PMMoV-I infected plants as well as for the changes in the Chl-FI parameters.

Acknowledgments We are grateful to María Teresa Serra (CIB, CSIC, Madrid) for the generous gift of PMMoV-I coat protein antiserum; to Greet Clerx, Jan Daenen and Natascha Steffanie for skilful technical assistance (Limburgs Universitair Centrum), as well as to Carlota Sajnani and Mónica Pineda (EEZ, CSIC, Granada) for their encouraging discussions providing their most recent data in the *N. benthamiana*-PMMoV system. This work was supported by the Spanish Ministry of Science and Technology, Ministry of Science and Education (Grants BIO2001-1937-C02 and BIO2004-04968-C02), Comunidad Autónoma de Madrid (CAM) and the BOF Funds of the Slimme Region of the Province of Limburg. MLPB was the recipient from a MCyT fellowship.

References

Almási A, Ekés M, Gáborjányi R (1996) Comparison of ultrastructural changes of *Nicotiana benthamiana* infected with three different tobamoviruses. Acta Phytopath et Entomol Hung 31:181–190

Almási A, Harsányi A, Gáborjányi R (2001) Photosynthetic alterations of virus-infected plants. Acta Phytopath et Entomol Hung 36:15–29

Alonso E, García-Luque I, Avila-Rincón MJ, Wicke B, Serra MT, Díaz-Ruiz JR (1989) A tobamovirus causing heavy losses in protected pepper crops in Spain. J Phytopathol 125:67–76

Baker NR, Rosenqvist E (2004) Applications of chlorophyll fluorescence can improve crop production strategies: an examination of future possibilities. J Exp Bot 55:1607–1621

Balachandran S, Osmond CB, Daley PF (1994) Diagnosis of the earliest strain-specific interactions between tobacco mosaic virus and chloroplasts of tobacco leaves in vivo by means of chlorophyll fluorescence imaging. Plant Physiol 104:1059–1065

Balachandran S, Osmond CB (1994) Susceptibility of tobacco leaves to photoinhibition following infection with two strains of tobacco mosaic virus under different light and nitrogen nutrition regimes. Plant Physiol 104:1051–1057

Balachandran S, Hull RJ, Martins RA, Vaadia Y, Lucas WJ (1997) Influence of environmental stress on biomass partitioning in transgenic tobacco plants expressing the movement protein of tobacco mosaic virus. Plant Physiol 114:475–481

Ball SG, Morell MK (2003) From bacterial glycogen to starch: understanding the biogenesis of the plant starch granule. Annu Rev Plant Biol 54:207–233

Barón M, Rahoutei J, Lázaro JJ, García-Luque I (1995) PSII response to biotic and abiotic stress. In: Mathis P (ed) Photosynthesis: from light to biosphere IV. Kluwer Academic Publishers, Dordrecht, pp 897–900

Beck E, Ziegler P (1989) Biosynthesis and degradation of starch in higher plants. Annu Rev Plant Physiol Plant Mol Biol 40:95–117

Berger S, Papadopoulos M, Schreiber U, Kaiser W, Roits T (2004) Complex regulation of gene expression, photosynthesis and sugar levels by pathogen infection in tomato. Physiol Plant 122:419–428

Björn LO, Forsberg AS (1979) Imaging by delayed light emission (phytoluminography) as a method for detecting damage to the photosynthetic system. Physiol Plant 47:215–222

Chaerle L, Van Der Straeten D (2001) Seeing is believing: imaging techniques to monitor plant health. Biochim Biophys Acta 1519:153–166

Chaerle L, Hagenbeek D, De Bruyne E, Valcke R, Van Der Straeten D (2004) Thermal and chlorophyll-fluorescence imaging distinguish plant–pathogen interactions at an early stage. Plant Cell Physiol 45:887–896

Cheng NH, Su CL, Carter SA, Nelson RS (2000) Vascular invasion routes and systemic accumulation patterns of tobacco mosaic virus in *Nicotiana benthamiana*. Plant J 23:349–362

Chou HM, Bundock N, Rolfe SA, Scholes JD (2000) Infection of *A. thaliana* leaves with *Albugo candida* (white blister rust) causes a reprogramming of host metabolism. Mol Plant Pathol 2:99–113

Ciscato M (2000) Development of a fluorescence imaging system for the quality asessment of fruit and vegetables. Limburg Universitair Centrum, Diepenbeek, Belgium

Cohen J, Loebenstein G (1974) An electron microscopy study of starch lesions in cucumber cotyledons infected with tobacco mosaic virus. Phytopathology 65:32–39

Critchley C, Russell AW (1994) Photoinhibition of photosynthesis in vivo: the role of protein turnover in photosystem II. Physiol Plant 92:188–196

Daley PF, Raschke K, Ball JT, Berry JA (1989) Topography of photosynthetic activity of leaves obtained from video images of chlorophyll fluorescence. Plant Physiol 90:1233–1238

del Rio LA, Pastori GM, Palma JM, Sandalio LM, Sevilla F, Corpas FJ, Jimenez A, Lopez-Huertas E, Hernandez JA (1998) The activated oxygen role of peroxisomes in senescence. Plant Physiol 116:1195–1200

Esau K, Cronshaw J (1967) Relation of tobacco mosaic virus to the host cells. J Cell Biol 33:665–678

Esfeld P, Siebke K, Weis E (1995) Local defence-related shift in the carbon metabolism in chickpea leaves induced by a fungal pathogen. In: Mathis P (ed) Photosynthesis: from light to biosphere V. Kluwer Academic Publishers, Dordrecht, pp 663–666

Fenton MJ, Crofts RA (1990) Computer-aided fluorescence imaging of photosynthetic systems: application of video imaging to the study of fluorescence induction in green plants and photosynthetic bacteria. Photosynth Res 26:59–66

Fryer MJ, Oxborough K, Mullineaux PM, Baker NR (2002) Imaging of photo-oxidative stress responses in leaves. J Exp Bot 53:1249–1254

Genty B, Meyer S (1994) Quantitative mapping of leaf photosynthesis using chlorophyll fluorescence imaging. Aust J Plant Physiol 22:277–289

Goodman RN, Király Z, Woods RK (1986) Photosynthesis. In: Biochemistry and physiology of plant disease. University of Missouri Press, Columbia, pp 46–74

Havelda Z, Maule AJ (2000) Complex spatial responses to cucumber mosaic virus infection in susceptible *Cucurbita pepo* cotyledons. Plant Cell 12:1975–1986

Holmes FO (1931) Local lesions of mosaic in *Nicotiana tabacum* L. Contrib Boyce Thompson Inst 3:163–172

Horton P, Wentworth M, Ruban A (2005) Control of the light harvesting function of chloroplast membranes: the LHCII-aggregation model for non-photochemical quenching. FEBS Lett 579:4201–4206

Hull R (2002) Matthew's plant virology. Academic Press, San Diego

Karpinski S, Gabrys H, Mateo A, Karpinska B, Mullineaux PM (2003) Light perception in plant disease defence signalling. Curr Opin Plant Biol 6:390–396

Lawson T, Oxborough K, Morison JI, Baker NR (2002) Responses of photosynthetic electron transport in stomatal guard cells and mesophyll cells in intact leaves to light, CO_2, and humidity. Plant Physiol 128:52–62

Lehto K, Tikkanen M, Hiriart JB, Paakkarinen V, Aro EM (2003) Depletion of the photosystem II core complex in mature tobacco leaves infected by the flavum strain of tobacco mosaic virus. Mol Plant Microbe Interact 16:1135–1144

Leipner J, Oxborough K, Baker NR (2001) Primary sites of ozone-induced perturbations of photosynthesis in leaves: identification and characterization in *Phaseolus vulgaris* using high-resolution chlorophyll fluorescence imaging. J Exp Bot 52:1689–1696

Lichtenthaler HK (1996) Vegetation stress: an introduction to the stress concept plants. J Plant Physiol 148:4–14

Lichtenthaler HK, Lang M, Sowinska M, Summ P, Miehe JA (1997) Uptake of the herbicide diuron as visualised by the fluorescence imaging technique. Bot Acta 110:158–163

Lindner RC, Kirpatrick HC, Weeks TE (1959) Some factors affecting the susceptibility of cucumber cotyledons to infection by tobacco mosaic virus. Phytopatology 49:78–88

Lohaus G, Heldt HW, Osmond CB (2000) Infection with phloem limited Abutilon mosaic virus causes localized carbohydrate accumulation in leaves of *Abutilon striatum*: relationships to

symptom development and effects on chlorophyll fluorescence quenching during photosynthetic induction. Plant Biol 2:161–167

Maliga P, Klessig DF, Cashmore AR, Gruissem W, Varner JE (1995) Methods in plant molecular biology: a laboratory manual. Cold Spring Harbor Lab Press, Cold Spring Harbor, NY

Meyer S, Saccardt AK, Rizza F, Genty B (2001) Inhibition of photosynthesis by *Colletotrichum lindemuthianum* in bean determined by chlorophyll fluorescence imaging. Plant Cell Environ 24:947–955

Ning LE, Gerald E, Edwards G, Strobel A, Larry S, Daley LS, Callis JM (1995) Imaging fluorometer to detect pathological and physiological changes in plants. Appl Spectrosc 49:1381–1389

Osmond CB, Daley PF, Badger MR, Lüttge U (1998) Chlorophyll fluorescence quenching during photosynthetic induction in leaves of *Abutilon striatum* Dicks infected with *Abutilon* mosaic virus observed with a field-portable system. Bot Acta 111:390–397

Ouzounidou G, Moustakas M, Eleftheriou EP (1997) Physiological and ultrastructural effects of cadmium on wheat (*Triticum aestivum* L.) leaves. Arch Environ Contam Toxicol 32:154–160

Oxborough K, Baker NR (1997) An instrument capable of imaging chlorophyll-alpha fluorescence from intact leaves at very-low irradiance and at cellular and subcellular levels of organization. Plant Cell Environ 20:1473–1483

Peltier G, Cournac L (2002) Chlororespiration. Annu Rev Plant Biol 53:523–550

Peterson RB, Aylor DE (1995) Chlorophyll fluorescence induction in leaves of *Phaseolus vulgaris* infected with bean rust (*Uromyces appendiculatus*). Plant Physiol 108:163–171

Pérez-Bueno ML, Rahoutei J, Sajnani C, García-Luque I, Barón M (2004) Proteomic analysis of the oxygen-evolving complex of photosystem II under biotic stress: studies on *Nicotiana benthamiana* infected with tobamoviruses. Proteomics 4:418–425

Pérez-Bueno ML (2003) Photosystem II and viral infection: analysis of fluorescence imaging and regulation of the synthesis of the oxygen-evolving-complex proteins during pathogenesis. Universidad de Granada, Granada, Spain

Rahoutei J, García-Luque I, Cremona C, Barón M (1998) Effect of tobamovirus infection on PSII complex of infected plants. In: Garab G (ed) Photosynthesis: mechanisms and effects IV. Kluwer Academic Publishers, The Netherlands, pp 2761–2764

Rahoutei J, Barón M, García-Luque I, Droppa M, Neményi A, Horvath G (1999) Effect of tobamovirus infection on the thermoluminiscence characteristics of chloroplast from infected plants. Z Naturforsch 54c:634–639

Rahoutei J, Garcia-Luque I, Baron M (2000) Inhibition of photosynthesis by viral infection: effect on PSII structure and function. Physiol Plant 110:286–292

Roberts AG, Cruz SS, Roberts IM, Prior D, Turgeon R, Oparka KJ (1997) Phloem unloading in sink leaves of *Nicotiana benthamiana*: comparison of a fluorescent solute with a fluorescent virus. Plant Cell 9:1381–1396

Rolfe SA, Scholes JD (1995) Quantitative imaging of chlorophyll fluorescence. New Phytol 131:69–79

Ruban AV, Horton P (1995) Regulation of non-photochemical quenching of chlorophyll fluorescence in plants. Aust J Plant Physiol 22:221–230

Ruiz del Pino M, Moreno A, García de Lacoba M, Castillo-Lluva S, Gilardi P, Serra MT, García-Luque I (2003) Biological and molecular characterization of P101 isolate, a tobamoviral pepper strain from Bulgaria. Arch Virol 148:2115–2135

Sajnani C, Pérez-Bueno ML, Pineda M, García-Luque I, Nedbal L, Benedikty M, Roncel M, Ortega JM, Ducruet JM, Römer S, Barón M (2005) The chloroplast as target of biotic stress: damage and defence during viral pathogenesis. In: van der Est A, Bruce D (eds) Photosynthesis: fundamental aspects to global perspective. ACG Publishing, Lawrence, KS

Scholes JD, Rolfe SA (1996) Photosynthesis in localised regions of oat leaves infected with crown rust (*Puccinia coronata*): quantitative imaging of chlorophyll fluorescence. Planta 199:573–582

Soukupová J, Smatanová S, Nedbal L, Jegorov A (2003) Plant response to destruxins visualized by imaging of chlorophyll fluorescence. Physiol Plant 118:399–405

Técsi LI, Maule AJ, Smith AM, Leegood RC (1994) Complex, localized changes in CO_2 assimilation and starch content associated with the susceptible interaction between cucumber mosaic virus and cucurbit host. Plant J 5:837–847

Técsi LI, Smith AM, Maule AJ, Leegood RC (1996) A spatial analysis of physiological changes associated with infection of cotyledons of marrow plants with cucumber mosaic virus. Plant Physiol 111:975–985

Valcke R, Ciscato M, Heisel F, Miehe J, Sowinska M (1999) Analysis of heavy-metal stressed plants by fluorescence imaging. In: Kamerman GW, Werner C (eds) Proc SPIE, 13th Annual International Symposium on Aerosense 3707:82–90, Orlando

van Wijk KJ, Schnettger B, Graf M, Krause GH (1993) Photoinhibition and recovery in relation to heterogeneity of Photosystem II. Biochim Biophys Acta 1142:59–68

Wetter C, Conti M, Alschuh D, Tabillion R, van Regemortel MHV (1984) Pepper mild mottle virus, a tobamovirus infecting pepper cultivars in Sicily. Phytopathology 74:405–410

Wright DP, Baldwin BC, Shephard MC, Scholes JD (1995) Source–sink relationships in wheat leaves infected with powdery mildew. I. Alterations in carbohydrate metabolism. Physiol Mol Plant Pathol 47:237–253

Wright DP, Baldwin BC, Shephard MC, Scholes JD (1995) Source–sink relationships in wheat leaves infected with powdery mildew. II. Changes in the regulation of the Calvin cycle. Physiol Mol Plant Pathol 47:255–267

Zeeman SC, Smith SM, Smith AM (2004) The breakdown of starch in leaves. New Phytol 163:247–261